ChemPhotoChem

Research Article
doi.org/10.1002/cptc.202500027

Chemistry Europe
European Chemical Societies Publishing

www.chemphotochem.org

Photooxygenation Reactions of Olefins Under Flow Conditions: An Experimental and *In-Silico* Study

Giada Moroni,[a, d] Yi-Hsuan Tsai,[b] Marco Ballarotto,[a, e] Andrea Carotti,[a] Jean-Christophe M. Monbaliu,*[b, c] and Antimo Gioiello*[a]

The photooxygenation reaction of olefins was investigated in a LED flow reactor module from both experimental and *in-silico* point of view. Initially, operating parameters potentially affecting the photoreaction efficiency, including the loading of the photosensitizer (methylene blue) (mol%), residence time and temperature were screened. The optimal conditions were then applied for the synthesis of 1,2-dioxetanes providing a straightforward and scalable approach to important chemiluminescent molecular probes for bioanalytical and diagnostic applications. Moreover, the scope of the reaction was tested for the oxidation of diverse alkenes under Schenck ene conditions leading synthetically useful hydroperoxides. From this, a chemometric analysis was performed to propose a preliminary *in-silico* model useful to both rationalize and predict the photooxygenation reaction outcome.

Introduction

Modern sustainability criteria in chemical synthesis have spurred the development of energy- and resource-conservative methodologies. Photooxygenations, which rely exclusively on abundant oxygen and visible light irradiation, have gained tremendous attention as one of the most atom-economic and sustainable reactions. Among the wide diversity of photooxidations, [2 + 2]-cycloadditions and the Schenck ene reaction use alkenes to provide 1,2-dioxetanes and allyl hydroperoxides, respectively (Figure 1). Both these reactions are endowed with a perfect atom economy and yield versatile synthetic precursors and chemical biology tools. 1,2-Dioxetanes are strained heterocycles with an increasing importance for bioanalytical and diagnostic applications as functional subunits of chemiluminescent probes (Figure 1C).[1,2] Similarly, allyl hydroperoxides are useful precursors to functionalized C3 units including natural products and drugs, such as artemisin and merucathine (Figure 1B).[3]

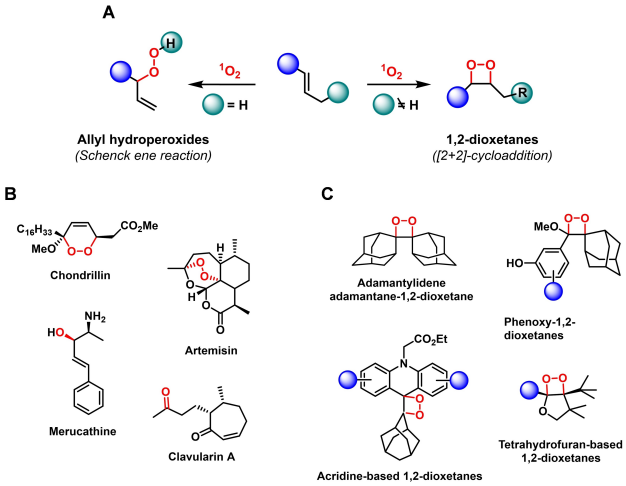

Figure 1. A) Photooxygenation reaction of alkenes to allyl hydroperoxides and 1,2-dioxetanes. B) Naturally occurring products and drugs synthesized from allyl hydroperoxides. C) Representative examples of 1,2-dioxetane-based chemiluminescent compounds.

Both reactions are promoted by singlet oxygen ($^1O_2$) that is formed *via* dye-sensitized photoexcitation of triplet oxygen ($^3O_2$).[4] $^1O_2$ is an attractive reactive oxygen species and it has been used for the synthesis of natural products, fragrances and drugs.[5,6] Photochemical singlet oxygenations can be problematic under conventional batch conditions. Especially at large scale, light penetration remains superficial and the presence of an oxygen-rich headspace in the presence of flammable organic solvents rises significant safety issues. Under flow conditions,

[a] *Dr. G. Moroni, Dr. M. Ballarotto, Prof. A. Carotti, Prof. A. Gioiello*
Laboratory of Medicinal and Advanced Synthetic Chemistry (Lab MASC)
Department of Pharmaceutical Sciences
University of Perugia
Via del Liceo 1, 06123 Perugia, Italy
E-mail: antimo.gioiello@unipg.it

[b] *Dr. Y.-H. Tsai, Prof. J.-C. M. Monbaliu*
Center for Integrated Technology and Organic Synthesis (CiTOS)
MolSys Research Unit, University of Liège
Allée du Six Août 13, 4000 Liège (Sart Tilman), Belgium
E-mail: jc.monbaliu@uliege.be

[c] *Prof. J.-C. M. Monbaliu*
WEL Research Institute
Avenue Pasteur 6, 1300 Wavre, Belgium

[d] *Dr. G. Moroni*
*Current address:*Institute of Applied Synthetic Chemistry
TU Wien
Getreidemarkt 9/163, BI EG G10, 1060 Vienna, Austria

[e] *Dr. M. Ballarotto*
*Current address:*Centre for Cancer Drug Discovery
The Institute of Cancer Research
SM2 5NG, London, UK

Supporting information for this article is available on the WWW under https://doi.org/10.1002/cptc.202500027

not only are the safety and light penetration aspects drastically improved, but the gas-liquid mass transfer is also significantly enhanced.[7] Indeed, the interfacial area that is essential for an efficient mass transfer rate of gas-liquid reactions is significantly higher in flow reactors than conventional batch equipment.[8]

Moreover, gas delivery can be tightly controlled, also when high pressures are needed to aid the dissolution of low soluble gases. Scale-up operations can potentially be easier by numbering-up reactors or through prolonged processing. Both approaches can drastically reduce the transition time moving to scale with obvious economic benefits. Recent achievements made in the combination of flow chemistry with LED light sources have offered novel options for improving safety and controlling the emitted light spectrum, enabling energy-savings while increasing efficiency (yields) and selectivity.[9] Several studies emphasizing the significant improvements of photochemical singlet oxygenations under flow conditions, as well as pilot-scale flow generators were recently documented.[10] The use of oxygen in flow photochemistry for cycloaddition and the Schenck ene reaction has been reported in literature for the preparation of the anthelmintic ascaridole by [4+2]-cycloaddition reaction of α-terpinene,[11] and for the oxidation of citronellol using supercritical CO_2 as reaction medium.[12]

In this work, we report a novel continuous flow photochemical process to 1,2-dioxetanes, thereby allowing a robust access to strained heterocycles such as spiroadamantane derivatives that are in the spotlight as chemical probes for bioanalytical and cell imaging applications.[13] Standard protocols for their preparation consist in the adoption of Kopecky method using hydrogen peroxide (H_2O_2) and 5,5-dimethyl-1,3-dibromohydantoin followed by silver-catalysed cyclization of the thus formed β-bromohydroperoxide.[14] $^1O_2$ addition is a more sustainable and efficient alternative, although under standard batch conditions the reaction is affected by a low reproducibility and batch-size dependency thus allowing the preparation of small quantities (10–50 mg) of product. Due to the aforementioned limitations, a more robust and efficient synthesis of the 1,2-dioxetanes should be developed to enable the preparation of new challenging dioxetane luminophores that can be screened for their light emission properties. Moreover, a series of functionalized alkenes were oxidized under Schenck ene flow conditions allowing the understanding of the reactivity profile toward the formation of products arising from competing hydrocarbon, alkene, and arene oxidations. Finally, a chemometric analysis was also conducted in an attempt to rationalize the observed photooxygenation reactivity and to provide a model that can predict the reactivity of other molecules of interest.

Results and Discussion

Reaction Screening and Flow Setup

Our interest in the development of acridine-containing 1,2-dioxetane-based bioanalytical probe[13e] led us to seek for more convenient protocols for their preparation under continuous flow conditions. To this aim, a DIY flow reactor connected to LED technology was designed and assembled (Figure S1, *Supporting Information*). A preliminary optimization was undertaken on model alkene **1a** in our DIY setup in order to frame the boundary conditions for our system (Scheme 1). The selection of the reaction solvent was crucial to guarantee the solubility of all reaction components, reactive oxygen species lifetime, and a simple scale-up.[15] Accordingly, CH_2Cl_2 was selected as the reaction solvent as it ensures a long $^1O_2$ lifetime and the complete solubility of reaction components, such as the sensitizer, preventing the reactor clogging and undesired light scattering.

The feed solution of olefin **1a** and a variable amount of methylene blue (MB) were dissolved in CH_2Cl_2 and were conveyed to a syringe pump (P) at different flow rates (Scheme 1). The solution was mixed *via* a T-shape mixer with a stream of O_2 controlled by a mass flow controller (MFC) and pumped into a reactor coil (R1) (V = 2.5 mL) irradiated with 610 nm LEDs at different temperatures. The O_2 flow rate has been initially set to ensure slugs flow with small and comparable size segments between O_2 and solvent. The moles of O_2 used in the reaction were calculated using formula (**I**).[10c]

$$(I)\ nO_2 = \frac{P_N(\text{atm})\ V_N(L)}{\text{R}(\text{L}\cdot\text{atm}\cdot mol^{-1}\cdot K^{-1})T_N(K)}$$

Back pressure regulators (BPRs) were inserted at the outlets of MFC (40 psi) and reactor (70 psi). Then, the crude was filtered through a small pad of silica gel (5 mm layer) or charcoal by using CH_2Cl_2 as eluent and the solution was concentrated at room temperature under vacuum. Using this flow setup, a number of experiments were carried out as reported in Table 1. Conversion and product yields, as well as the formation of decomposition products were determined by ^{1}H-NMR analysis of crude reaction mixtures (Figure S2, *Supporting Information*).

As expected, both temperature and reaction time strongly influenced the reaction outcome and, as seen, the formation of decomposition products **3a** and **4** (Scheme 1). In particular, reactions carried out at −5 °C gave a lower decomposition rate in comparison to 25 °C (Table 1, *entry 1 vs 2*). Moreover, a

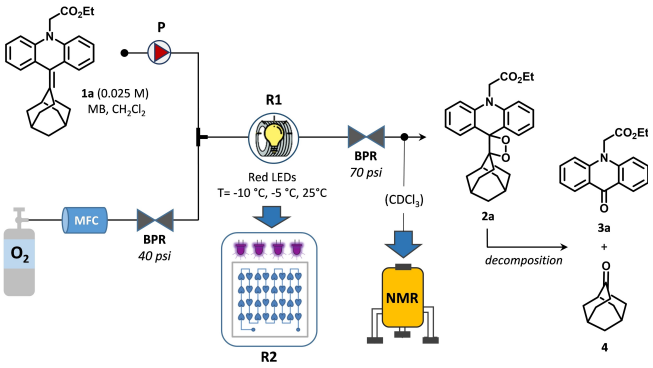

Scheme 1. General flow setup for the photooxygenation of compound **1a** chosen as the model substrate. BPR: back pressure regulator; MFC: mass flow controller; P: syringe pump; R1: reactor coil irradiated with red LEDs (610 nm); R2: glass module irradiated with red LEDs (610 nm).

Table 1. Preliminary reaction screening under flow conditions using compound **1a** as the model substrate.[a]

Entry	MB (%)	P flow rate (mL min^{-1})	O_2 flow rate (mL min^{-1})	T (°C)	Conversion (%)[b]	2a (%)[b]	Decomposition products (%)[b]
1	6	0.2	2	25	>99	44	56
2	6	0.2	2	−5	>99	66	34
3	6	1.25	12.5	−5	>99	94	6
4	1	1.25	12.5	25	82	68	14
5	1	1.25	12.5	−5	94	91	3
6	6	1.25	12.5	−10	78	75	3

[a] All reactions were performed on 20 mg scale. [b] Determined by ^{1}H-NMR analysis of the crude reaction mixtures.

shorter residence time improved selectivity by maintaining the same conversion while reducing the thermal decomposition of dioxetane **2a** (*entry 2 vs 3*). However, lower temperatures (i.e., −10 °C) led to low conversion (*entry 6*), and decreasing the amount of photosensitizer also resulted in less conversion (*entry 4–5*). The best results were obtained at −5 °C using 6 mol% of photosensitizer to get a complete consumption of the starting material in only 50 seconds, excellent yield (94%) with only traces of the decomposition products (6%), and a productivity of 1.4 g h^{-1} (Table 1, *entry 3*). It is worth noting that the reaction conducted under batch mode (MB = 6 mol%, T = −5 °C, t = 1 h) was batch-size dependent affording the desired dioxetane product **2a** in only 34% yield, despite the quantitative conversion yield.

Next, the photooxygenation conditions were transposed to a commercial mesofluidic photoreactor equipped with one glass module (R2) (2.6 mL irradiated internal volume) and two thermostated LED panels (Scheme 1). When the best reaction conditions from the DIY device were transposed to this system, decomposition products **3a** and **4** were formed in a much larger extent (Table 2, *entry 1*).

We hypothesized that such extensive decomposition was related to the higher irradiation intensity achieved in the commercial mesofluidic system. Consequently, the intensity of the lamp was gradually decreased to reach the best compromise between conversion to target product and photodegradation (*entries 2 and 3*). The photoreaction was further optimized by reducing both the O_2 flow rate and the amount of photosensitizer. *Entry 5* showed the best conditions in terms of yield (97%) and productivity (600 mg h^{-1}), within only 2 min of residence time. Increasing the concentration of the feed solution to 0.1 M (Table 2, *entry 6*) led to incomplete conversion. We assume that, even if the LED power is similar in both setups, the flat-stacked configuration (with LED panels mounted on both sides of the fluidic glass module) in the commercial reactor ensured a more uniform irradiation, leading to a higher photon flux density. Additionally, the static heart-shaped mixers integrated throughout the glass module of the commercial reactor improve gas-liquid mixing, enhanced photooxidation performance compared to the homemade PFA coil setup.

Substrate Scope

With an unprecedented flow protocol to access 1,2-dioxetanes in hands, we sought to expand the scope using a set of commercially available and synthesized olefins. Initially, we commenced to develop an efficient protocol for the generation of adamantyl 1,2-dioxetanes.[13] Using the optimal protocol and setup, the reaction was attempted on diverse adamantyl-containing olefins **1b–d**, **5a–h** (Table 3–4).

In particular, we focused our attention on the nature of the endocyclic heteroatom and replaced the nitrogen atom of compound **1a** with oxygen and sulphur (Table 3, *entries 3 and 4*). The oxygen-bearing compound **1c** underwent photooxygenation allowing us to obtain the corresponding 1,2-dioxetane **2c** in high yield (88%). The sulphur-containing olefin **1d** did not react with singlet oxygen probably due to steric and

Table 2. Reaction screening and optimization for the photooxygenation of compound **1a** in a commercial mesofluidic photoreactor.[a]

Entry	MB (%)	P flow rate (mL min^{-1})	O_2 flow rate (mL min^{-1})	O_2:1a ratio[b]	LED intensity (%)	Conversion (%)[c]	**2a** (%)[c]	Decomposition products (%)[c]
1	6	1.25	12.5	11:1	100	>99	80	20
2	6	1.25	12.5	11:1	50	>99	88	12
3	6	1.25	12.5	11:1	10	>99	93	7
4	6	1.25	1.25	1:1	10	>99	92	8
5	3	1.25	1.25	1:1	10	>99	97	3
6	3	1.25	1.25	1:1	10	65	60	5

[a] All reactions were performed under LED irradiation at 610 nm on 20 mg scale except for entry 6 (64 mg scale, 0.1 M). [b] Determined according to equation **I**. [c] Determined by ^{1}H-NMR analysis of the crude reaction mixture.

Table 3. Photooxygenation reaction of adamantane-containing tricyclic aromatic olefins under flow conditions.[a]

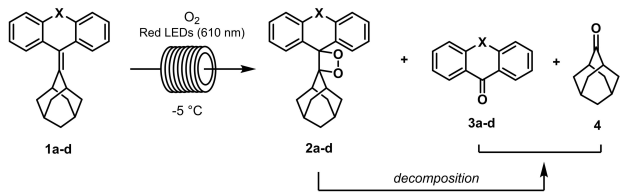

Entry	Olefin	X	Conversion (%)[b]	**2a–d** (%)[b]	Decomp. products (%)[b]
1	**1a**	NCH_2CO_2Et	>99	94	6
2	**1b**	–	78	28	50
3	**1c**	O	92	88	4
4	**1d**	S	–	–	–

[a] Stock solution: olefin **1a–d** (25 mM) and MB (3 mol%) in CH_2Cl_2. The solution was pumped at 1.25 mL min^{-1} and the O_2 was pumped at 12.5 mL min^{-1}. The mixture was irradiated with red LEDs (610 nm) and temperature of the reactor was set at −5 °C. [b] Determined by ^{1}H-NMR analysis of the crude reaction mixture. The solvent was evaporated under vacuum and the crude was dissolved in $CDCl_3$.

Table 4. Photooxygenation reaction of adamantane-containing olefins under flow conditions.[a]

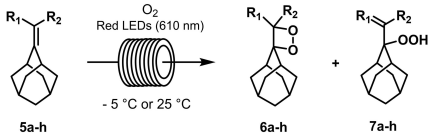

Entry	Olefin	R_1, R_2	Convers. (%)[b]	**6a–d** (%)[b]	**7a–g** (%)[b]
1	**5a**	OMe, Ph	>99%	98	–
2	**5b**	Adamantyl	>99%	>99%	–
3	**5c**	H, Ph	–	–	–
4	**5d**	Me, Ph	>99%	–	>99%
5	**5e**	Me, 4F-Ph	>99%	–	>99%
6	**5f**	Me, 4Me-Ph	>99%	–	>99%
7	**5g**	Me, 4OMe-Ph	>99%	–	>99%
8	**5h**	H, H	–	–	–

[a] Stock solution: olefin **5a–h** (25 mM) and MB (3 mol%) in CH_2Cl_2. The solution was pumped at 1.25 mL min^{-1} and the O_2 was pumped at 12.5 mL min^{-1}. The mixture was irradiated with red LEDs (610 nm) and temperature of the reactor was set at −5 °C or 25 °C. [b] Determined by ^{1}H-NMR analysis of the crude reaction mixture. The solvent was evaporated under vacuum and the crude was dissolved in $CDCl_3$.

electronic factors, while the reaction was acceptable on fluorene compound **1b** (Table 3, *entry 2*).

Thermally stable 1,2-dioxetanes including the methoxyphenyl (**6a**) and adamantylideneadamantane 1,2-dioxetane (*Adox*, **6b**) were obtained in excellent yield, avoiding the formation of the corresponding epoxides that can be formed as major by-products (Table 4, *entries 1 and 2*).[16] As expected, alkenes **5d–g** bearing allylic hydrogens gave ene-addition reaction furnishing the corresponding hydroperoxides **7d–g** in quantitative yield. In all these cases, the reaction can be performed both at −5 °C and 25 °C in view of the relative thermal stability of the products formed. Conversely, olefins **5c** and **5h** failed to react under our conditions.

A second set of alkenes consisted in a series of endocyclic olefins (**8a–f**) (Table 5). As expected, electron-rich alkenes favoured the photooxygenation.[17] Indeed, olefin **8b** which has two electron donating groups attached to the double bond, yielded a greater formation of dioxetane in comparison to its analogue **8a**, which bears only one methyl group. However, the selectivity of the reaction with these two olefins was decreased by competing ene-reactions owing to the presence of allylic protons. It should be pointed out that O_2/olefin ratio, flow rate and LED intensity was found to have significant effect on the reaction outcome and product formation (see also Table S1–2, *Supporting Information*). Consistent with previous findings,[17] enhanced rigidity of the double-bond system, exemplified by compound **8c**, seems to favour the selectivity toward dioxetane formation. Moreover, the heterocycle nature carrying the double bond may also influence the reaction outcome with singlet oxygen. In this regard, benzofurans may promote [2+2]-cycloadditions compared to indenes, as evidenced by the difference between **8a**, **8b**, and **8c** *vs* **8d**.

As an example of the enhanced performance of dioxetane formation in flow, we may consider compound **8d**. In a previous report on batch photooxygenation, using the more expensive tetraphenylporphyrin (TPP) as a photosensitizer at −10 °C for 3 h, a 53% isolated yield of the desired dioxetane was obtained.[18] In contrast, our flow-based method, with an estimated residence time of 47 seconds at −5 °C, achieved a complete conversion. Although only 40% of the product was the desired dioxetane, we anticipate that operating at lower temperatures may prevent dioxetane decomposition leading to higher yields. Additionally, our method has the advantages of using a more cost-effective photosensitizer (MB) and significantly reducing reaction time.

Next, the reaction was attempted on thermally stable dioxetanes bearing a phenylethenyl (**12**) and phenylethynyl moiety (**14**) (Scheme 2).[20] The reaction provided dioxetanes **13** and **15** in 24% and 39% yield, respectively, along with the corresponding decomposition products (ketoesters, 5–6%). It is important to note that although **12** can undergo [4+2]-cycloaddition of singlet oxygen with the conjugated diene

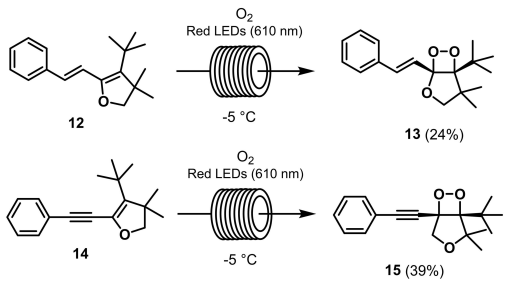

Scheme 2. Photooxygenation reaction of phenylethenyl- (**12**) and phenylethynyl-substituted dihydrofuran (**13**) under flow conditions.

Table 5. Photooxygenation reaction of endocyclic olefins under flow conditions.[a]

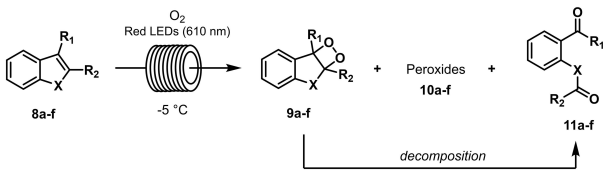

Entry	Olefin	X	R_1	R_2	Conversion (%)[b]	Product ratio (%)[b]		
						9a–f	**10a–f**	**11a–f**
1	**8a**	CH_2	H	CH_3	85	–	81	4
2	**8b**	CH_2	CH_3	CH_3	>99	30[19]	57	17
3	**8c**	CH_2	Ph	Ph	69	–	–	69
4	**8d**	O	CH_3	CH_3	>99	40	23	37
5	**8e**	CH_2CH_2	H	H	59	–	59	–
6	**8f**	CH_2	H	Ph	<5	n.d.	n.d.	n.d.

[a] Stock solution: olefin **8a–f** (25 mM) and MB (3 mol%) in CH_2Cl_2. The solution was pumped at 1.25 mL min^{-1} and the O_2 was pumped at 12.5 mL min^{-1}. The mixture was irradiated with red LEDs (610 nm, intensity 100%) and temperature of the reactor was set at −5 °C. [b] Average of three fractions, determined by ^{1}H-NMR analysis of the crude reaction mixture. The solvent was evaporated under vacuum and the crude was dissolved in $CDCl_3$. n.d. = not determined.

system, and 1,2-addition to the styryl double bond, only dioxetane **13** was observed.

Other olefins such as styrene (**16a**), *E*-1,2-diphenylethene (**16b**), and *E*-1,2-diphenylethene (**16c**) failed to provide the corresponding 1,2-dioxetanes under different reaction conditions (MB mol%: 1–6, O_2 flow rate: 2–12.5 mL min^{-1}) (*data not shown*).

In summary, these results evidenced that electron-rich alkenes are mainly converted into 1,2-dioxetanes, while when alkenes are characterized by allylic hydrogens, the ene-addition leading to hydroperoxides can be the major or competitive reaction.[21] Moreover, the nature of the olefin substituents (electron-donating ability, presence of hydrogen-bond acceptors and/or donors, geometry, and steric hindrance) not only affects the success of singlet oxygen addition, but it also determines the reaction pathway.

In-Silico Analysis

A comprehensive quantum mechanical description of the photooxygenation process can give valuable information on the observed experimental trends. However, it is a demanding and time-consuming task, which generally requires computationally expensive levels of theory and several different reaction pathways to be considered.[22] We have therefore adopted a simple chemometric approach based on a single *ab-initio* calculation applied on the starting structure. With respect to previously reported protocols,[13e,23] scaffold-specific geometric descriptors (interatomic distances and dihedral angles) were discarded to gather experimental data from a larger chemical structural domain, stepping towards the development of a general photooxygenation model. Thus, we consider only electronic descriptors consisting of the HOMO and LUMO energy of the molecule, and the Mulliken partial charges together with the atomic contribution to HOMO and LUMO of the atoms involved in the reaction.

All the molecules were subjected to a molecular mechanics conformational search performed with Macromodel package present in the Schrodinger Suite 2023-1.[24] Subsequently, all conformers within 6 kcal/mol from the minimum recorded energy underwent a DFT geometry optimization at the B3LYP/6-31G(d) level of theory (*see Supporting Information* for further details). Next, we extracted the abovementioned descriptors from the lowest-energy conformer and analyzed all the tested olefins submitted to the flow photooxygenation process. Before the model development, all the descriptors were scaled and centred. The calculated descriptors can be found in Table S7–S8 in the *Supporting Information* and as a csv files as *Supporting data*.

A principal component analysis (PCA) was performed on the dataset using three principal components (PCs). The resulting model was able to explain 73.6% of the total variance within the first three PC, explaining the 32.3%, 24.8% and 19.8% of the variance for the first, second and third PC, respectively. Although a clear clustering of the reactive and unreactive olefins cannot be identified, a certain degree of separation between the two classes is present in the PCs scatter plots (Figure 2).

This observation prompted us to delve deeper into a more quantitative chemometric investigation and to perform a classification task using the linear discriminant analysis (LDA) technique on the full olefin dataset comprising of 16 reactive and 7 unreactive molecules by using the previously calculated descriptors (Table S9, *Supporting Information*). The resulting model was able to perfectly discriminate the two reactivity classes (Figure 3, mean scores of reactive class: −1.09, mean scores of unreactive class: 2.48). Moreover, the developed

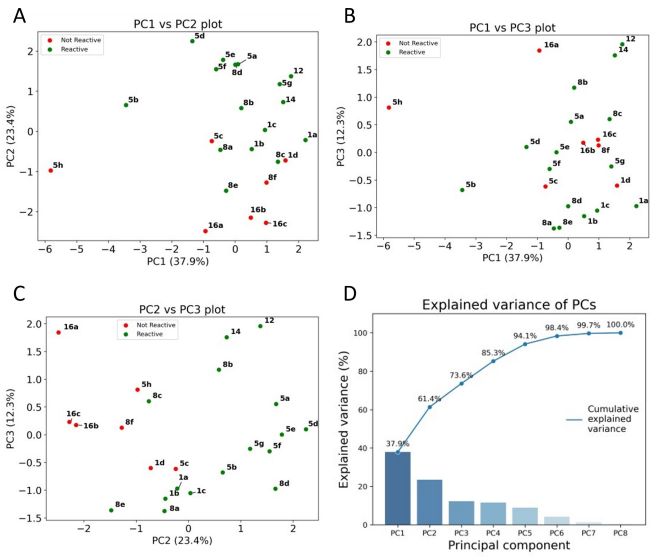

Figure 2. Plots of the PCA on the full dataset. A) 3D plot of PC1 *vs* PC2 *vs* PC3. B) PC1 *vs* PC2 plot. C) PC1 *vs* PC3 plot. D) Explained variance of the Principal Components.

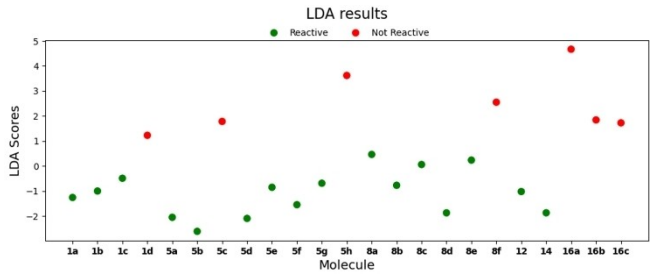

Figure 3. Linear discriminant analysis (LDA) results on the full olefin dataset.

model was found to be quite robust even after accounting for the significant class imbalance, as highlighted by the high mean accuracy during Leave-One-Out Cross-Validation (mean accuracy: 91 %, accuracy standard deviation: 28 %).

In order to further test the robustness of the model in predicting photooxygenation reactivity of organic molecules, we used a test set composed by 40 acridine-based olefins (28 reactive and 12 unreactive) taken from previously published papers.[13e,22] We were pleased to find that the developed model was able to accurately predict the reactivity of 85 % of the test set (34 molecules out of 40), despite the underrepresentation of this chemical class in the training dataset (Figure 4). Indeed, among the olefins presented in this work, only less than 20 % are of the "acridine-like" class (4 out of 23, compounds **1 a**–**d**). Notably, a large portion of the compounds that were incorrectly predicted as reactive shared structural elements that could lead to radical side-reactions or quenching of the photocatalyst (benzylic positions and naphthyl moiety, respectively).

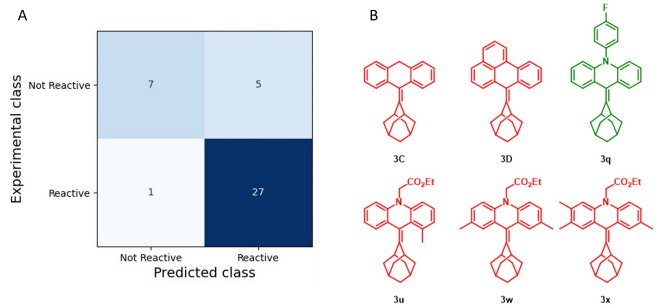

Figure 4. LDA reactivity prediction results on the test set. A) Confusion matrix of the predictions from the LDA model. B) Structures of the incorrectly predicted compounds. The color refers to the experimental class (red = not reactive, green = reactive). The compound numbering refers to ref. [13e,22].

Conclusions

With the move towards innovative and sustainable chemistry, the use of metal oxidants such as chromium and permanganate in oxidation reactions has been replaced by oxygen, either alone or in combination with catalysts. In this context, continuous flow oxygenation reactions have been applied in several manufacturing processes and laboratory synthesis of high-value chemicals and drugs.

In this work, we have studied the efficiency of photo-oxygenation reaction under flow conditions. The developed methodology has been tested on a series of olefins including important chemiluminescent 1,2-dioxetane probes. The scope of this flow protocol is wide since several olefins were successfully reacted to afford both 1,2-dioxetanes and hydro-peroxides. We expect that this new flow photooxygenation approach would be particularly useful to facilitate the gram scale preparation of known dioxetane-based chemiluminescent substrates as well as to enable the access to highly challenging, new and yet unexplored chemiluminescent luminophores. Furthermore, we have investigated the potential of our flow protocol to allylic photooxidation (Schenck ene reaction) towards diverse sets of allyl hydroperoxides, crucial precursors of fine chemical building blocks and bioactive compounds. Finally, an *in-silico* model has been proposed to rationalize and predict the conversion at the reactor outlet. In the future, this starting model can be improved by additional data from literature and easily adopted by other laboratories for the same scope.

Experimental Section

Flow Photooxygenation Reaction of Ethyl 2-(9-((5R,7R)-adamantan-2-ylidene)acridin-10(9H)-yl)acetate (1 a)

A syringe pump from Syrris ltd equipped with Asia red syringes was used to convey the feed solution of olefin **1 a** and MB dissolved in CH_2Cl_2 into the Corning® Advanced-Flow™ Lab Photo Reactor. The gas flow rate was controlled with a Bronkhorst® F210C™ mass flow controller (MFC). A Zaiput Flow Technologies® dome-type back-pressure regulator (BPR) was inserted downstream and connected

to a cylinder of compressed nitrogen (set point: 5.6 bar). The reactor was maintained at reaction temperature with a LAUDA Integral XT 280 thermostat while LAUDA® Proline RP 845™ thermostat was used for the thermoregulation of the mesofluidic reaction glass module and the LED illumination setup at 15 °C using silicone oil as coolant. LED panels were mounted on both sides of the fluidic module (40 mm from the centre of the reaction path). Each LED panel was equipped with multiple wavelengths (20 LEDs for 6 wavelengths) with wireless intensity control.

Ethyl 2-((5″R,7″R)-10*H*-dispiro[acridine-9,3′-[1,2]dioxetane-4′,2″-adamantan]-10-yl)acetate (2a). Yield: 97%. Yellow solid. ^{1}H-NMR (400 MHz, $CDCl_3$): δ = 0.62 (d, 2H, J = 12.4 Hz), 1.15 (d, 2H, J = 12.4 Hz), 1.27 (t, 3H, J = 7.1 Hz), 1.37–2.07 (m, 8H), 2.28 (s, 2H), 4.28 (q, 2H, J = 7.08 Hz), 4.65 (s, 2H), 6.81–6.83 (m, 2H), 7.18–7.22 (m, 2H), 7.35–7.39 (m, 2H), 8.20–8.22 (m, 2H). ^{13}C-NMR (100.6 MHz, $CDCl_3$): δ = 14.2, 17.4, 25.4, 25.6, 26.9, 31.7, 32.8, 32.9, 36.1, 39.2, 48.4, 61.6, 86.8, 97.8, 111.8, 121.0, 121.6, 128.4, 129.1, 139.1, 169.2.

Computational Analysis

The computational workflow was adapted from previously published works.[13e,22] The training and test set molecules were drawn with Schrodinger's Maestro software suite 2023-1.[23] All Molecular Mechanics (MM) calculations were performed with the Macromodel module of the Maestro software suite 2023-1.[24] All DFT calculations were performed with Gaussian 09 (Revision D.01). The molecules were then subjected to a MM conformational search using the MMFF94 force field as implemented in the software. The conformational search was performed using a mixed torsional/low-mode sampling, optimizing the resulting geometries with the Polak-Ribier Conjugate Gradient (PRCG) algorithm converging on a gradient threshold of 0.05 kJ mol^{-1} Å^{-1}. All the found conformers within 6 kcal/mol from the lowest-laying conformer were kept and underwent DFT geometry optimization at the B3LYP/6-31G(d) level of theory. The lowest-energy conformer from the DFT optimization was then used to calculate the molecular descriptors used in this work. The electronic descriptors were obtained directly from the Gaussian output file. The atoms of the double bond involved in the reaction were numbered based on their Mulliken partial charges, with the atom with the highest charge numbered as 1. The HOMO and LUMO energies were converted to eV prior to the analysis. All the computational data analysis was performed using an in-house Python (v. 3.7.0) script. The dataset composed of the extracted descriptors was then scaled and centred. PCA and LDA analyses were performed with using the scikit-learn module (v. 0.22.1), while all plots were drawn with matplotlib (v. 3.5.1) and seaborn (v. 0.12.2).

Acknowledgements

This project was supported by the National Recovery and Resilience Plan (NRRP), Mission 4, Component 2, Investment 1.1, Call for tender No. 104 published on 2.2.2022 by the Italian Ministry of University and Research (MUR), funded by the European Union – NextGenerationEU – Project Title "Thermochemiluminescence-based nanoprobes for multiplex prostate cancer biomarkers in personalized medicine (THERMOPROS)" – CUP J53D23007580006. We also would like to thank Giovanni Battista Minotti and Andrea Nicoziani for their help with the preparation of olefin substrates and realization of the first prototype of photochemical reactor, respectively. Open Access publishing facilitated by Università degli Studi di Perugia, as part of the Wiley - CRUI-CARE agreement.

Conflict of Interests

The authors declare no conflict of interest.

Data Availability Statement

The data that support the findings of this study are available in the supplementary material of this article.

Keywords: 1,2-dioxetanes · chemometrics · flow chemistry · photooxygenation · Schenck ene reaction

[1] M. Matsumoto, *J. Photochem. Photobiol. C* **2004**, *5*, 27–53.
[2] H. Wynberg, E. W. Meijer, J. C. Hummelen, in *Methods in enzymology*, Vol. 57 (Eds.: M. A. DeLuca, W. D. McElroy), Academic Press Inc., **1981**, pp. 687–689.
[3] P. Bayer, R. Pérez-Ruiz, A. J. von Wangelin, *ChemPhotoChem* **2018**, *2*, 559–570.
[4] C. Schweitzer, R. Schmidt, *Chem. Rev.* **2003**, *103*, 1685–1758.
[5] A. A. Ghogare, A. Greer, *Chem. Rev.* **2016**, *116*, 9994–10034.
[6] V. Nardello-Rataj, P. L. Alsters, J.-M. Aubry, in *Liquid phase aerobic oxidation catalysis: Industrial applications and academic perspectives*, Chapter 22 (Eds.: S. S. Stahl, P. L. Alsters), Wiley-VCH Verlag GmbH & Co. KGaA, **2016**, pp. 369–395.
[7] a) C. Sambiagio, T. Noël, *Trends Chem.* **2020**, *2*, 92–106; b) D. Cambié, C. Bottecchia, N. J. W. Straathof, V. Hessel, T. Noël, *Chem. Rev.* **2016**, *116*, 10276–10341; c) J. P. Knowles, L. D. Elliott, K. I. Booker-Milburn, *Beilstein J. Org. Chem.* **2012**, *8*, 2025–2052.
[8] C. J. Mallia, I. R. Baxendale, *Org. Process Res. Dev.* **2016**, *20*, 327–360.
[9] a) M. Oelgemöller, N. Hoffman, *Org. Biomol. Chem.* **2016**, *14*, 7392–7442; b) M. Pagliaro, *Chem. Today* **2017**, *35*, 84–85.
[10] a) Y.-H. Tsai, M. Cattoen, G. Masson, G. Christen, L. Traber, M. Donnard, F. R. Leroux, G. Bentzinger, S. Guizzetti, J.-C. M. Monbaliu, *React. Chem. Eng.* **2024**, *9*, 1646–1655; b) N. Emmanuel, P. Bianchi, J. Legros, J.-C. M. Monbaliu, *Green Chem.* **2020**, *22*, 4105–4115; c) N. Emmanuel, C. Mendoza, M. Winter, C. R. Horn, A. Vizza, L. Dreesen, B. Heinrichs, J.-C. M. Monbaliu, *Org. Process Res. Dev.* **2017**, *21*, 1435–1438; d) R. Radjagobalou, J.-F. Blanco, O. Dechy-Cabaret, M. Oelgemöller, K. Loubière, *Chem. Engineer. Proc.: Proc. Intensif.* **2018**, *130*, 214–228; e) C. Y. Park, Y. J. Kim, H. J. Lim, J. H. Park, M. J. Kim, S. W. Seoa, C. P. Park, *RSC Adv.* **2015**, *5*, 4233–4237; f) K. Kaya-Özkiper, K. Mc Carogher, A. Roibu, S. Kuhn, *ACS Sustainable Chem. Eng.* **2023**, *11*, 9761–9772; g) R. Bannon, G. Morrison, M. Smyth, T. S. Moody, S. Wharry, P. M. C. Roth, G. Gauron, M. Baumann, *Org. Process Res. Dev.* **2024**, *28*, 3307–3312.
[11] C. Mendoza, N. Emmanuel, C. A. Páez, L. Dreesen, J.-C. M. Monbaliu, B. Heinrichs, *ChemPhotoChem* **2018**, *2*, 890–897.
[12] a) R. A, Maurya, C. P. Park, D.-P. Kim, *Beilstein J. Org. Chem.* **2011**, *7*, 1158–1163; b) F. Levesque, P. H. Seeberger, *Org. Lett.* **2011**, *13*, 5008–5011; c) F. Levesque, P. H. Seeberger, *Angew. Chem. Int. Ed.* **2012**, *51*, 1706–1709.
[13] a) N. Hananya, D. Shabat, *Angew. Chem. Int. Ed.* **2017**, *56*, 16454–16463; b) O. Green, S. Gnaim, R. Blau, A. Eldar-Boock, R. Satchi-Fainaro, D. Shabat, *J. Am. Chem. Soc.* **2017**, *139*, 13243–13248; c) O. Green, T. Eilon, N. Hananya, S. Gutkin, C. R. Bauer, D. Shabat, *ACS Cent. Sci.* **2017**, *3*, 349–358; d) T. Nobeshima, M. Nakakomi, K. Nakamura, N. Kobayashi, *Adv. Opt. Mater.* **2014**, *1*, 144–149; e) G. Moroni, D. Calabria, A. Quintavalla, M. Lombardo, M. Mirasoli, A. Roda, A. Gioiello, *ChemPhotoChem* **2022**, *6*, e202100152; f) Y. L. Chen, A. J. H. Spiering, S. Karthikeyan, G. W. M. Peters, E. W. Meijer, R. P. Sijbesma, *Nat. Chem.* **2012**, *4*, 559–562; g) E. W. Meijer, H. Wynberg, *Tetrahedron Lett.* **1979**, *20*, 3997–4000; h) L. De Vico, Y. J. Liu, J. W. Krogh, R. Lindh, *J. Phys. Chem. A* **2007**, *111*, 8013–8019; i) D. J. Vinyard, S. Su, M. M. Richter, *J. Phys. Chem. A* **2008**, *112*(37), 8529–8533.

[14] a) K. R. Kopecky, J. E. Filby, C. Mumford, P. A. Lockwood, J.-Y. Ding, *Can. J. Chem.* **1975**, *53*, 1103–1122; b) K. R. Kopecky, C. Mumford, *Can. J. Chem.* **1969**, *47*, 709–711.
[15] P. Bayera, A. J. von Wangelin, *Green Chem.* **2020**, *22*, 2359–2364.
[16] a) T. Hirano, C. Matsuhashi, *J. Photochem. Photobiol., C: Photochem. Rev.* **2022**, *51*, 100483; b) J. H. Wieringa, J. Strating, H. Wynberg, W. Adam, *Tetrahedron Lett.* **1972**, *13*, 169–172.
[17] K. Gollnick, K. Knutzen-Mies, *J. Org. Chem.* **1991**, *56*, 4017–4027.
[18] W. Adam, O. Albrecht, E. Feineis, I. Reuther, C. R. Saha-Möller, P. Seufert-Baumbach, D. Wild, *Liebigs Ann. Chem.* **1991**, *1991*, 33–40.
[19] The area under the corresponding pick was not well solved. This justifies that the sum of all products percentages exceeds 100%.
[20] M. Matsumoto, T. Ishihara, N. Watanabe, T. Hiroshima, *Tetrahedron Lett.* **1999**, *40*, 4571–4574.
[21] E. L. Bastos, P. Farahani, E. J. H. Bechara, W. J. Baader, *J. Phys. Org. Chem.* **2017**, *30*, e3725.
[22] a) M. Bobrowski, A. Liwo, S. Ołdziej, D. Jeziorek, T. Ossowski, *J. Am. Chem. Soc.* **2000**, *122*, 8112–8119; b) A. G. Leach, K. N. Houk, *Chem. Commun.* **2002**, 1243–1255.
[23] L. A. Andronico, A. Quintavalla, M. Lombardo, M. Mirasoli, M. Guardigli, C. Trombini, A. Roda, *Chem. Eur. J.* **2016**, *22*, 18156–18168.
[24] Schrodinger Release 2023–1, Macromodel v13.9, Schrödinger, LLC, New York, NY, **2023**.
[25] Schrodinger Release 2023–1, Macromodel v13.9, Schrödinger, LLC, New York, NY, **2023**.

Manuscript received: January 29, 2025
Accepted manuscript online: February 13, 2025
Version of record online: February 26, 2025